2814 *Chem. Mater.* **2010,** *22,* 2814–2821
DOI:10.1021/cm903740e

CHEMISTRY OF MATERIALS
Article

CdSe Quantum Rod Formation Aided By In Situ TOPO Oxidation

Abraham Wolcott, Robert Carl Fitzmorris, Omed Muzaffery, and Jin Z. Zhang*

Department of Chemistry and Biochemistry, University of California, Santa Cruz, California 95064

Received December 14, 2009. Revised Manuscript Received March 12, 2010

In situ TOPO decomposition was accomplished by applying a vacuum at elevated temperatures to a precursor solution in the presence of oxygen, leading TOPO to oxidize to di-*n*-octylphosphinic acid (DOPA) and octylphosphonic acid (OPA). The mixed-ligand system of tetradecylphosphonic acid (TDPA), DOPA, and OPA produced CdSe QRs on the order of 4 nm in diameter and 20 nm in length. Solvent and ligand identification was performed by mass spectrometry and ^{31}P nuclear magnetic resonance spectroscopy. Transmission electron microscopy (TEM) was utilized to determine the morphology, size, and crystal growth of the CdSe QRs. This method of CdSe QR synthesis is unique in that the phosphonic acids responsible for anisotropic growth are formed in situ, prior to the nucleation and growth of the nanorods. Without the oxidation of TOPO, CdSe quantum dots (QDs) were synthesized instead, as reported previously. This discovery reinforces the efficacy of DOPA and OPA molecules as critical ligands in the formation of one-dimensional (1D) nanostructures.

Introduction

Semiconductor nanoparticles (NPs), nanorods (NRs), and heterostructures have been widely studied for their unique electronic, photophysical, and transport properties, as well as for their use in devices.[1−14] Advancements in wet chemical synthesis techniques have led to homogeneous size distributions, high quantum yields and safer precursor materials. Growth mechanisms of CdSe quantum rods and CdTe tetrapods have been explained by the preferential attachment of ligands to certain crystal facets, precursor concentration levels and temperature dependent crystal phase growth.[8,11] Anisotropic growth of unique crystal facets leads to 1D nanostructures of varying diameter and length. Nanomaterials spanning a broad range of dimensions and sizes have been fervently examined over the past decade. Their unique optical properties inherent in quantum confined systems have lent these materials to be utilized in biological labeling, optoelectronics, and photovoltaic cells.[15−22] High degrees of synthetic control are necessary for both fundamental and device investigations, but the mechanisms of nanocrystal growth are not completely understood.

Currently, the understanding of crystal growth mechanisms of nanomaterials can be broken down into four parts: (1) initial nucleation based on critical concentration precipitation, (2) monomer diffusion and addition to nucleated sites, (3) ligand preferential binding characteristics, and (4) inherent crystal facet potential energy.[23−26] A recent in situ TEM study also points to NP-NP coalescence as a driving force in NP growth kinetics.[27] Nanocrystal

*Corresponding author. E-mail: zhang@chemistry.ucsc.edu.

(1) Alivisatos, A. P.; Harris, T. D.; Brus, L. E.; Jayaraman, A. *J. Chem. Phys.* **1988**, *89*, 5979.
(2) Bawendi, M. G.; Carroll, P. J.; Wilson, W. L.; Brus, L. E. *J. Chem. Phys.* **1992**, *96*, 946.
(3) Bawendi, M. G.; Wilson, W. L.; Rothberg, L.; Carroll, P. J.; Jedju, T. M.; Steigerwald, M. L.; Brus, L. E. *Phys. Rev. Lett.* **1990**, *65*, 1623.
(4) Brus, L. *Isr. J. Chem.* **1993**, *33*, 9.
(5) Chestnoy, N.; Hull, R.; Brus, L. E. *J. Chem. Phys.* **1986**, *85*, 2237.
(6) Marcus, M. A.; Flood, W.; Stiegerwald, M.; Brus, L.; Bawendi, M. *J. Phys. Chem.* **1991**, *95*, 1572.
(7) Huynh, W. U.; Dittmer, J. J.; Alivisatos, A. P. *Science* **2002**, *295*, 2425.
(8) Manna, L.; Scher, E. C.; Alivisatos, A. P. *J. Am. Chem. Soc.* **2000**, *122*, 12700.
(9) Ryan, K. M.; Mastroianni, A.; Stancil, K. A.; Liu, H. T.; Alivisatos, A. P. *Nano Lett.* **2006**, *6*, 1479.
(10) Scher, E. C.; Manna, L.; Alivisatos, A. P. *Philos. Trans. R. Soc. London, Ser. A* **2003**, *361*, 241.
(11) Manna, L.; Milliron, D. J.; Meisel, A.; Scher, E. C.; Alivisatos, A. P. *Nat. Mater.* **2003**, *2*, 382.
(12) Hu, J. T.; Ouyang, M.; Yang, P. D.; Lieber, C. M. *Nature* **1999**, *399*, 48.
(13) Duan, X. F.; Huang, Y.; Cui, Y.; Wang, J. F.; Lieber, C. M. *Nature* **2001**, *409*, 66.
(14) Gradecak, S.; Qian, F.; Li, Y.; Park, H. G.; Lieber, C. M. Appl. Phys. Lett. **2005**, *87*.
(15) Bruchez, M.; Moronne, M.; Gin, P.; Weiss, S.; Alivisatos, A. P. *Science* **1998**, *281*, 2013.
(16) Gerion, D.; Pinaud, F.; Williams, S. C.; Parak, W. J.; Zanchet, D.; Weiss, S.; Alivisatos, A. P. *J. Phys. Chem. B* **2001**, *105*, 8861.
(17) Wolcott, A.; Gerion, D.; Visconte, M.; Sun, J.; Schwartzberg, A.; Chen, S. W.; Zhang, J. Z. *J. Phys. Chem. B* **2006**, *110*, 5779.
(18) Kim, S.; Lim, Y. T.; Soltesz, E. G.; De Grand, A. M.; Lee, J.; Nakayama, A.; Parker, J. A.; Mihaljevic, T.; Laurence, R. G.; Dor, D. M.; Cohn, L. H.; Bawendi, M. G.; Frangioni, J. V. *Nat. Biotechnol.* **2004**, *22*, 93.
(19) Kazes, M.; Lewis, D. Y.; Ebenstein, Y.; Mokari, T.; Banin, U. *Adv. Mater.* **2002**, *14*, 317.
(20) Kamat, P. V. *J. Phys. Chem. C* **2008**, *112*, 18737.
(21) Law, M.; Beard, M. C.; Choi, S.; Luther, J. M.; Hanna, M. C.; Nozik, A. J. *Nano Lett.* **2008**, *8*, 3904.
(22) Luther, J. M.; Law, M.; Beard, M. C.; Song, Q.; Reese, M. O.; Ellingson, R. J.; Nozik, A. J. *Nano Lett.* **2008**, *8*, 3488.
(23) Murray, C. B.; Norris, D. J.; Bawendi, M. G. *J. Am. Chem. Soc.* **1993**, *115*, 8706.
(24) Peng, X. G.; Wickham, J.; Alivisatos, A. P. *J. Am. Chem. Soc.* **1998**, *120*, 5343.
(25) Talapin, D. V.; Rogach, A. L.; Shevchenko, E. V.; Kornowski, A.; Haase, M.; Weller, H. *J. Am. Chem. Soc.* **2002**, *124*, 5782.
(26) Manna, L.; Wang, L. W.; Cingolani, R.; Alivisatos, A. P. *J. Phys. Chem. B* **2005**, *109*, 6183.
(27) Zheng, H. M.; Smith, R. K.; Jun, Y. W.; Kisielowski, C.; Dahmen, U.; Alivisatos, A. P. *Science* **2009**, *324*(5932), 1309–1312.

Published on Web 04/15/2010
© 2010 American Chemical Society

nucleation is typically understood as a supersaturation of precursor material in solution leading to an arrested precipitation state mediated by surfactants. This is accomplished by the quick injection of precursor materials into aqueous or organic solvents. Subsequent heating then facilitates growth by the addition of solubilized monomers that can then add to the nucleated cluster. Small clusters or "magic" size assemblies of II−VI semiconductors have been reported and their photophysical properties investigated.[28−31] These ultrasmall clusters are recognized by even further blue-shifted absorption and emission characteristics from their larger nanoparticle counterparts.

In going from zero-dimensional (0D) QDs to 1D QRs, ligand composition, and monomer concentration have been found to be critically important synthetically. An initial report on nanorod synthesis in 1999 included the use of only technical grade TOPO and quickly injected Cd and Se precursors dissolved in tributylphosphine.[32] Although the CdSe QRs were only 8 nm × 13 nm, it became apparent that anisotropic growth could be accomplished with the organometallic route as it had been with studies utilizing the vapor−liquid−solid (VLS) methods.[33] Impurities in the technical grade TOPO were the likely culprit in the formation of anisotropic 1D nanostructures. Technical grade TOPO at 90% purity was known to possibly include degraded phosphonic acids produced during synthesis due to side reactions. Various "batches" with different lengths of aging were discovered to produce either QDs or QRs with the same synthetic protocol. Later on, controlled CdSe QR growth was accomplished with the use of high purity TOPO, hexylphosphonic acid (HPA), or tetradecylphosphonic acid (TDPA).[8,34,35] High aspect ratios could then be more reproducibly achieved because of the precise control over the chemical composition of the reaction solution. Consequently, the synthetic irreproducibility inherent in using technical grade TOPO was then diminished because, the phosphonic acids responsible for nanocrystal growth were now controllably added to the organometallic solution. It should still be noted that even in 99% TOPO, 10 synthetic impurities have been identified, as will be discussed in more detail later.[36]

A number of theoretical studies have delved into the role of surfactants and their binding affinity to three major crystal facets of CdSe.[26,37−40] Ab initio calculations performed by Puzder et al. utilized density functional theory (DFT) on $Cd_{15}Se_{15}$ and $Cd_{33}Se_{33}$ clusters to understand the dynamics of QD and QR growth.[37] In their study they attached four ligands; phosphine oxide, phosphonic acid, carboxylic acid, and trimethylamine to the polar and apolar facets of wurtzite CdSe. The polar facets of 0001 and $000\bar{1}$ are the growth directions responsible for the anisotropic growth of CdSe QR (ends), while $01\bar{1}\ 0$ and $11\bar{2}\ 0$ are the apolar facets that represent the sides of an individual QR. Consequently the ab initio calculations showed that the binding energies of phosphine oxide and phosphonic acid were appreciably stronger on the apolar facets (∼1.23−1.45 eV) compared to the less-stable polar facets (∼0.63−1.11 eV). Binding was generally dominated by surfactant−Cd interactions, and it was found that surfactant molecules placed next to surface apolar Se atoms would quickly find their lowest energy state bound to a Cd site. The weaker binding affinity to the polar facets in turn means that the removal of that surfactant molecule will be easier, and addition of Cd and Se monomers will be accelerated.[26] Increased crystal facet growth velocities leads to the anistropic growth inherent in CdSe QRs along the weakly bound 001 growth directions. Interestingly, along the 0001Cd facet, it was found that 100% surfactant coverage would lead to a thermodynamically favorable removal of a surfactant molecule because of increased electron density on that facet.[26] These thermodynamic considerations reinforce how subtle changes in reaction conditions such as TOPO impurities can have drastic results on morphology.

TOPO has been the central solvent in the organometallic route for II−VI semiconductors and has revolutionized the standards for size dispersity, crystallinity, quantum efficiency, and morphology of quantum confined nanomaterials.[8,23,24,32,41,42] Recently, several studies have used NMR and MS analysis to precisely investigate the composition of TOPO/phosphinic/phosphonic acid-based CdSe nanocrystal synthesis.[36,43−45] Although it has been nearly a decade since the initial investigations of the connection between morphological control and impurities in technical grade TOPO began, only recently have some of the details began to emerge.[46] Wang et al. identified 10 common impurities found in 90% TOPO and 99% TOPO batches. Through thorough examination, they made the case that the relative ratio of

(28) Bowers, M. J.; McBride, J. R.; Rosenthal, S. J. *J. Am. Chem. Soc.* **2005**, *127*, 15378.
(29) Dagtepe, P.; Chikan, V.; Jasinski, J.; Leppert, V. J. *J. Phys. Chem. C* **2007**, *111*, 14977.
(30) Kudera, S.; Zanella, M.; Giannini, C.; Rizzo, A.; Li, Y. Q.; Gigli, G.; Cingolani, R.; Ciccarella, G.; Spahl, W.; Parak, W. J.; Manna, L. *Adv. Mater.* **2007**, *19*, 548.
(31) Riehle, F. S.; Bienert, R.; Thomann, R.; Urban, G. A.; Krugert, M. *Nano Lett.* **2009**, *9*, 514.
(32) Huynh, W. U.; Peng, X. G.; Alivisatos, A. P. *Adv. Mater.* **1999**, *11*, 923.
(33) Hu, J. T.; Odom, T. W.; Lieber, C. M. *Acc. Chem. Res.* **1999**, *32*, 435.
(34) Peng, Z. A.; Peng, X. G. *J. Am. Chem. Soc.* **2001**, *123*, 1389.
(35) Peng, Z. A.; Peng, X. G. *J. Am. Chem. Soc.* **2002**, *124*, 3343.
(36) Wang, F.; Tang, R.; Kao, J. L. F.; Dingman, S. D.; Buhro, W. E. *J. Am. Chem. Soc.y* **2009**, *131*, 4983.
(37) Manna, L.; Wang, L. W.; Cingolani, R.; Alivisatos, A. P. *J. Phys. Chem. B* **2005**, *109*, 6183.
(38) Puzder, A.; Williamson, A. J.; Zaitseva, N.; Galli, G.; Manna, L.; Alivisatos, A. P. *Nano Lett.* **2004**, *4*, 2361.
(39) Rempel, J. Y.; Trout, B. L.; Bawendi, M. G.; Jensen, K. F. *J. Phys. Chem. B* **2005**, *109*, 19320.
(40) Rabani, E. *J. Chem. Phys.* **2001**, *115*, 1493.
(41) Milliron, D. J.; Hughes, S. M.; Cui, Y.; Manna, L.; Li, J. B.; Wang, L. W.; Alivisatos, A. P. *Nature* **2004**, *430*, 190.
(42) Becerra, L. R.; Murray, C. B.; Griffin, R. G.; Bawendi, M. G. *J. Chem. Phys.* **1994**, *100*, 3297.
(43) Liu, H. T.; Owen, J. S.; Alivisatos, A. P. *J. Am. Chem. Soc.* **2007**, *129*, 305.
(44) Wang, F. D.; Tang, R.; Buhro, W. E. *Nano Lett.* **2008**, *8*, 3521.
(45) Peng, X. G.; Manna, L.; Yang, W. D.; Wickham, J.; Scher, E.; Kadavanich, A.; Alivisatos, A. P. *Nature* **2000**, *404*, 59.
(46) Kopping, J. T.; Patten, T. E. *J. Am. Chem. Soc.* **2008**, *130*, 5689.

impurities in various batches of TOPO (tech and high purity) either hinders, allows for, or has no effect on the synthesis of high-quality CdSe nanowires.[36,44] Of the impurities they highlighted, DOPA and OPA were recognized as key components in the successful growth of high-quality CdSe nanowires. Wang et al. justified DOPA's efficacy in CdSe nanowire growth by explaining that DOPA modifies the formation of CdSe through the ligand substitution of precursor materials. To test their theory, they added successive amounts of DOPA, OPA, and mono-*n*-octylphosphinic acid (MOPA) to examine the resulting quality of their CdSe nanowires. Additions of DOPA, OPA, and MOPA to medium and poor quality TOPO batches subsequently resulted in high-quality CdSe nanowire formation. Batches of commercially available TOPO that resulted in superior CdSe nanowire formation were understood to have beneficial amounts of DOPA.

In the present work, we reinforce that DOPA and OPA are also critical to the growth of much smaller, 4 nm × 20 nm CdSe QRs. In a deviation of Wang's work, we have identified that DOPA and OPA were produced when residual oxygen was allowed to persist in the reaction solution of CdO/TOPO/TDPA under a weak vacuum of 1000 mTorr, and a vacuum was applied at elevated temperatures of ~280−300 °C. In situ DOPA and OPA formation via TOPO oxidation were apparent because of a change in coloration of the solution and smoke formation, understood to be 1-octene degradation. The CdSe QRs and their precursor solutions were characterized with optical spectroscopy, electron microscopy, mass spectroscopy (MS), and nuclear magnetic resonance (NMR) spectroscopy.

Experimental Section

The CdSe QRs studied here were synthesized via a modified organometallic method in a coordinating solvent of TOPO and TDPA based on the work of Peng et al.[34,35,47] The CdSe QRs were produced in common "air-free" conditions on a nitrogen filled Schlenk line. Briefly, 50 mg of CdO (Acros Organics #22379, 99%), 4.1 g of TOPO (Strem Chemicals #15−6661, 99%), and 305 mg of TDPA (PCI synthesis # 4671−75−4, 99%) were placed in a 50 mL three neck flask with septa, thermocouple and refluxing column attached to the Schlenk line. To remove residual water and some oxygen from the mixture, the solution was heated to 120 °C under a nitrogen flow and subsequently placed under a weak vacuum. During the degassing process, the vacuum was held at 1000 mTorr or higher. This was done to ensure dissolved oxygen was significant enough to oxidize TOPO in an observable amount. A 0.16 M SeTOP solution was prepared in a nitrogen filled glovebox by placing 4 mL of technical grade tri-*n*-octylphosphine (Aldrich #117854, 90%) and 42.0 mg of Se powder (Acros Organics #19807, 99% 200 mesh) into a scintillation vial, capped with a septum and stirred vigorously. After removal from the glovebox, the SeTOP solution was sonicated for 30−45 s to ensure complete dissolution of the Se powder. The SeTOP solution was optically clear, colorless, and had no visible Se particles. After three nitrogen purge and vacuum cycles (≥1000 mTorr), the solution of CdO in TOPO/TDPA was optically clear with no color to a slight golden tint by 250 °C. Special care was taken that all CdO was completely dissolved and no residual CdO powder resided on the flask walls by vigorously shaking the vessel. At ~280−300 °C, the nitrogen flow was ceased and a weak vacuum was applied to the CdO/TOPO/TDPA solution. Smoke formed above the solution, the solution color changed to a darker golden hue, the vacuum was stopped, and a nitrogen flow was applied. Aliquots of the pre- and postoxidation steps were collected for MS and NMR analysis. With a solution temperature of 270 °C, 4.0 mL of the 0.16 M SeTOP was injected, and the solution temperature dropped to 230 °C. The injection needle was purged of oxygen prior to SeTOP addition by placing the syringe into the Teflon capped vial of SeTOP with a constant flow of nitrogen. Growth of the CdSe QRs was performed at 260 °C, and tracked via UV−vis spectroscopy and photoluminescence (PL) spectroscopy by extracting small aliquots from the reaction mixture into toluene. Growth was allowed to continue for 20 min, then allowed to cool to approximately 50 °C, 7 mL of toluene was injected and the QRs were then precipitated with 5−10 mL of methanol. Three precipitation and decantation cycles were performed by dispersing the QRs in toluene and precipitating with methanol. The CdSe QRs were ultimately left as a solid and then dissolved in toluene or chloroform as needed.

All UV−visible (UV−vis) absorption spectra were performed on a Hewlett-Packard 8452A diode array spectrophotometer (Palo Alto, CA). Photoluminescence (PL) spectroscopy was measured on a Perkin-Elmer LS 50B (Fremont, CA) with an excitation wavelength of 390 nm and 1% attenuator. Samples were placed in open sided 1 cm path length quartz cuvettes for both PL and UV−vis measurements. PL measurements were made with CdSe QR concentrations between 0.1 and 0.3 absorption units at 390 nm, and no normalization was used. Transmission electron microscopy (TEM) was carried out on a JEOL 1200 EX with a Gatan CCD and software. TEM and high resolution TEM images were obtained with a Phillips CM200/FEG (Field Emission Gun) microscope at the National Center for Electron Microscopy (NCEM) at Lawrence Berkeley National Laboratory in Berkeley, CA. ^{1}H and ^{31}P nuclear magnetic resonance (NMR) was carried out on samples dissolved in deuterated chloroform and experimentation was performed on a Varian Unity 500. Mass Spectroscopy (MS) was conducted by dissolving small amounts of the pre and postcombustion CdO/TOPO/TDPA solutions in methanol (ng/L) and data was collected on a Thermo Finnigan LTQ (San Jose, CA,). The MS had an electrospray injection system with a capillary temperature of 275 °C, a positive polarity of +4.5 kV and a negative polarity of −5.00 kV.

Results

CdSe Quantum Dot vs Quantum Rod Growth. Under normal reaction conditions without TOPO oxidation, CdSe QD formation would dominate as seen by Peng using CdO as a precursor.[47] If QD formation proceeded because of a failed TOPO oxidation, two distinct characteristics would prevail; (1) no smoking or change in coloration would be present to the precursor solution, and (2) the growth of the QD diameter would happen on faster time scales in comparison to QR formation. During the growth of either CdSe QDs or QRs, aliquots of the growth solution were dissolved in toluene, and utilized to track the nanocrystal growth via UV−vis absorption

(47) Peng, Z. A.; Peng, X. G. *J. Am. Chem. Soc.* **2001**, *123*, 183.

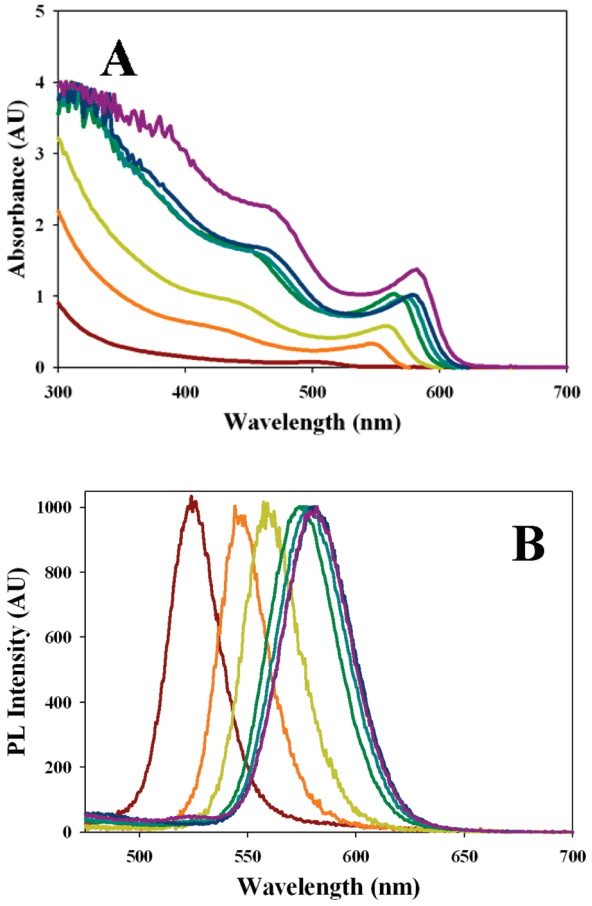

Figure 1. UV−vis absorption spectra showing the growth of CdSe nanorods from 2 to 20 min (A). Excitonic peak position red shifts as the inherent bandgap of the material becomes smaller in energy. PL spectra shows the consummate shifting of the bandedge emission as the CdSe nanorods are growing (B). The CdSe nanorods only display bandedge emission, and there are no apparent shallow or deep trap emissive states.

spectroscopy. First excitonic peak positions during a QD synthesis would take ~5 min to reach 575 nm. In contrast, during QR synthesis, it would take a 20 min growth period to evolve a first exciton peak to 575 nm. The bulk room temperature linear absorption and PL spectra of the CdSe QRs are shown in Figure 1. The first excitonic peak for quantum confined CdSe first appeared around 500 nm and continued to red shift until ca. 575−580 nm in the UV−vis spectra. Red-shifting of the excitonic peak is representative of the quantum confined CdSe QR diameter, and is not defined by the length of the QR. This continuous shifting is indicative of the dynamic increase of the QR diameter during the growth period at 260 °C. Therefore, Cd and Se monomers are being added to both the unique *c*-axis facet (polar facets 0001 and 000$\bar{1}$), and the facets representative of the QR diameter simultaneously (apolar 01$\bar{1}$ 0 and 11$\bar{2}$ 0 facets). As supported by Puzder and Manna, the phosphonic acids are more weakly bound to the polar facets, causing surfactant removal to happen more readily from the polar facet, thus allowing for faster addition of Cd and Se precursors.[26,37] Subsequently, the more tightly bound apolar facets passivated by phosphonic acids are still displaced due to the high temperature of the growth solution (260 °C), but allow for Cd and Se addition at a reduced rate. Similarly, the PL spectra displayed a red-shift in band-edge luminescence as the QRs were growing, and there were no indication of shallow/deep trap state emission. Raw QRs did display a blue-shifted emission shoulder (in relation to band-edge peak) prior to solution precipitation and resuspension (data not shown). The PL shoulder was understood to be emanating from spherical QDs in the ensemble that were later separated by the cleaning process. For the final QRs, the peak of the PL is Stokes-shifted from the absorption by approximately 7 nm from 575 to 582 nm and the PL band has a full-width at half-maximum (fwhm) of 35 nm. From the bulk absorption and PL measurements, an effective CdSe diameter of approximately 4 nm can be inferred.[48]

TEM images showed that the phosphonic acid capped CdSe QRs were ca. 4 nm × 20 nm, in good agreement with particle diameter as a function of excitonic peak position (Figure 2A). Although most of the CdSe QRs have an aspect ratio of 5:1, other nanostructures were also observed, including bipods, tripods and tetrapods that account for <5% of the products (see Figure S1 in the Supporting Information). The observation of bipods, tripods and tetrapods was first reported on by Manna et al., and later investigated thoroughly in the case of CdTe tetrapods.[8,11] Branching was observed in the ensemble of CdSe QRs and is believed to be due to the nature of the mixed ligand system and the varying alkyl chain length used to grow the CdSe QRs. A systematic study of CdSe QR growth as a function of varying the phosphonic acid alkyl chain length (6−18 carbon) reported branching percentages ranging from 0% with *n*-octadecylphosphonic acid to >99% when using hexylphosphonic acid.[49] Our surfactant system contains both 8 and 14 carbon chain phosphonic acids, leading to a moderate amount of branching (~25%). In our case, the mixed-ligand system produces nonuniform steric hindrance at the nanocrystal surface, as multiple molecular species compete for polar and apolar binding sites. Increased hydrophobic interactions from bound surfactant molecules to apolar facets should provide additional stabilization along the sides of the QR, thus reducing branching. Although theoretical studies show only minor binding energy changes (0.01 eV) between methyl and full chain phosphine oxides and phosphonic acids, experimental results show markedly different results.[37,49] Both steric affects and hydrophobic interactions may play some role in these discrepancies. HRTEM imaging reveals the lattice fringes of single-crystalline CdSe QRs, and a lattice constant of ~3.6 Å was measured along the long axis of the individual QR (Figure 2B). The lattice spacing of 3.57 Å is representative of the 001 crystal facet of wurtzite CdSe and is consistent with previous reports.[50] Dislocations and vacancies can also be seen in the HRTEM images of some of the representative CdSe QRs.

(48) Yu, W. W.; Qu, L. H.; Guo, W. Z.; Peng, X. G. *Chem. Mater.* **2004**, *16*, 560.
(49) Wang, W.; Banerjee, S.; Jia, S. G.; Steigerwald, M. L.; Herman, I. P. *Chem. Mater.* **2007**, *19*, 2573.
(50) Mokari, T.; Banin, U. *Chem. Mater.* **2003**, *15*, 3955.

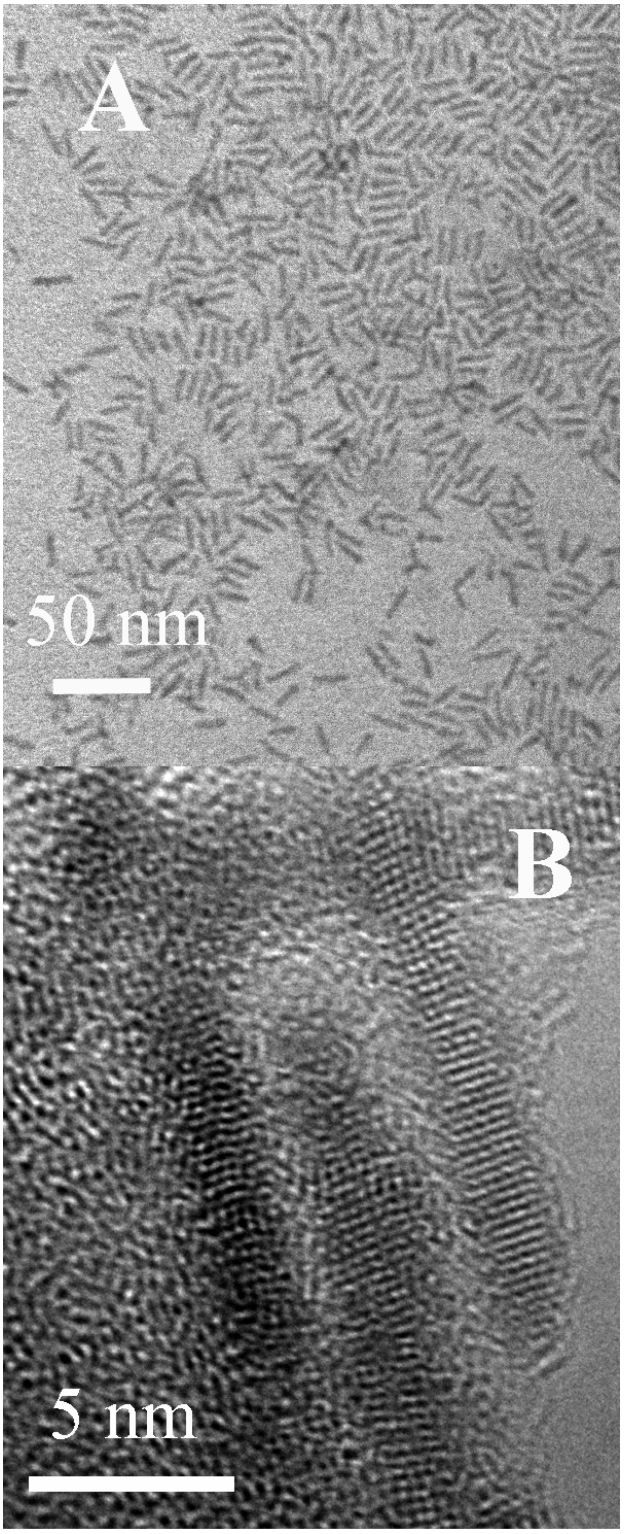

Figure 2. (A) TEM image of an ensemble of CdSe QRs with an approximate size of 4 nm ×20 nm. (B) HRTEM image of three CdSe QRs reveal the crystal lattice of wurtzite CdSe. The lattice constant along the unique *c*-axis was found to be 3.57 Å, representative of the 001 crystal facet. Dislocations and vacancies can be observed in the length of the CdSe QRs.

Identification of DOPA and OPA as the Main Products of TOPO Oxidation Following Smoking. In a typical synthesis of CdSe QDs, the three basic precursors, CdO, TOPO and TDPA are used in conjunction with a selenium trioctylphosphine (SeTOP) or selenium tributylphosphine (SeTBP) solution. By modifying the relative concentration of TDPA the controllable synthesis of QRs can be attained.[34,35] Prior to SeTOP or SeTBP injection, the precursor solution would typically be thoroughly degassed to remove bound water and oxygen. In our case, we allowed a weak vacuum of 1000 mtorr at 120−150 °C to take place during the degassing step. Due to the relatively weak vacuum, adsorbed oxygen remains present in the CdO/TOPO/TDPA solution. At elevated temperatures of 280−300 °C and in conjunction with an applied vacuum, resulted in a smoking of the solution, and a modification of the coloration of the solution from colorless→light golden hue or light golden hue→ darkened golden hue. This general change in the coloration was an obvious indicator of a chemical transformation taking place. During the oxidation of TOPO, four molecular species were produced: (1) DOPA, (2) 1-octene, (3) OPA, and (4) mono-*n*-octylphosphinic acid (MOPA). We believe the combustion of 1-octene is responsible for the smoking that was observed. Because the oxidation of TOPO was performed at 280−300 °C, the evolution of 1-octene is above the autoignition temperature of 230 °C, and was found to decompose rapidly. Initially, poorly controlled reactions of TOPO oxidation led to minor flames at the surface of the CdO/TOPO/TDPA during the applied vacuum, and were extinguished when the vacuum was ceased. MS and NMR spectra of preoxidation and postoxidation solutions were the general tool used to determine their molecular composition. Consequently, 1-octene was not readily identified using either experimental technique.

MS data of an aliquot of the preoxidation CdO/TOPO/TDPA solution in negative mode shows two major peaks (Figure 3A). The main peak is representative of TDPA at 277.25 mass/charge units and the second largest is at 289.27 representative of the molecule DOPA, and was mentioned previously as the major impurity in both tech and 99% TOPO batches.[36,44] The relative abundance of TDPA was considered 100%, and DOPA's relative abundance in comparison was 14%. The presence of DOPA prior to oxidation was reinforced by control TOPO samples that revealed the largest impurity to be DOPA (SOM/S2). The control TDPA MS data shows no other peaks than those representative of TDPA, and therefore we can conclude that any additional peaks prior to oxidation are caused by TOPO impurities (SOM/S3). In the original preoxidation solution, OPA was detected at a relative abundance of 0.75%, and could have been formed from minor TOPO oxidation at elevated temperatures. The drastic increase in relative OPA and DOPA concentration is evident after the oxidation step is applied.

Postoxidation MS data shows not only TDPA and DOPA peaks, but also the appearance of the OPA molecule produced during the oxidation step of the synthesis and a change in the relative abundance ratio of TDPA/DOPA (Figure 3B). Preoxidation data confirms that OPA was not significantly present (0.75%) in the Cd/TOPO/TDPA mixture, but was instead chemically produced at

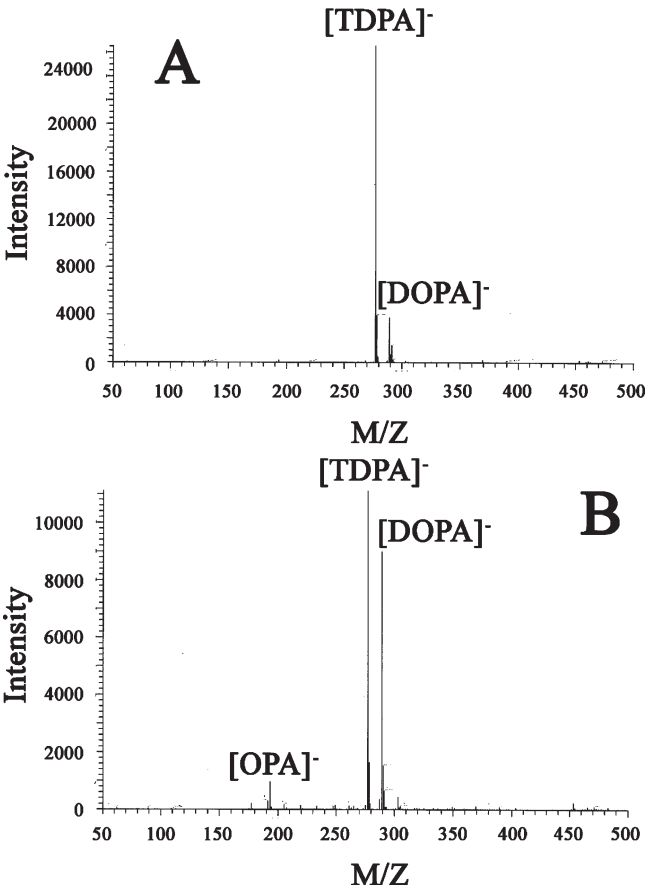

Figure 3. MS data of solutions of Cd/TOPO/TDPA precursor solutions (A) before and (B) after combustion. The data was taken with a negative polarity and specifically probed the phosphonic acids within the precursor solution. Most notably is the appearance of a peak at 193 M/Z, representative of octylphosphonic acid (OPA). Other peaks of special interest are the dimers of OPA at 387.02 and the TDPA+OPA dimer at 471.05. Di-*n*-octylphosphinic acid (DOPA) is also found in the pre- and post-combustion solutions at 289.41, which consequently did not show up in stock solutions of TDPA or TOPO.

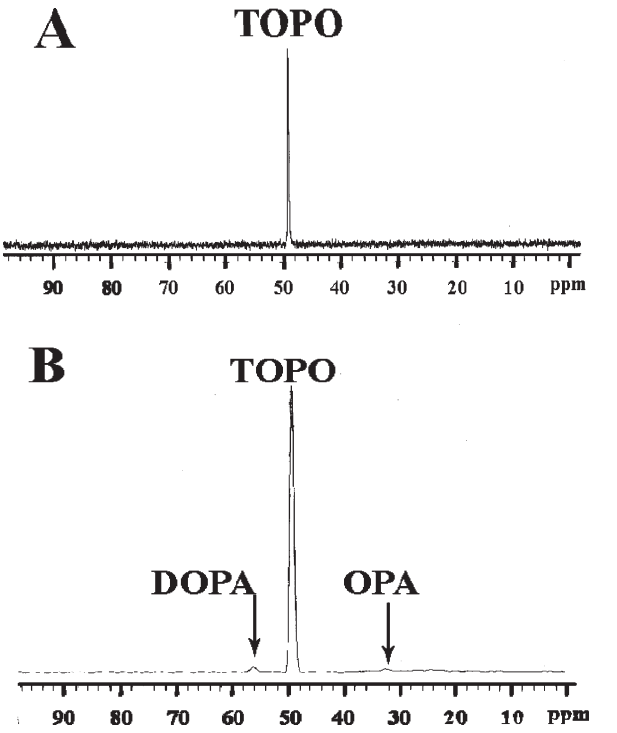

Figure 4. (A) ^{31}P NMR spectra showing the presence of only TOPO prior to the oxidative step with a representative peak at ~49.2 ppm. (B) After the oxidative step, peaks emerge at 56.2 and 32.5 ppm that have been identified as DOPA and OPA, respectively. Because of the relatively small amount of MOPA, it was not readily seen in the ^{31}P NMR spectra.

high temperature (280−300 °C), with residual oxygen and an applied vacuum. If during the initial degassing portion of the synthesis, the overall pressure became lower than ~1 Torr (120−150 °C), we would not observe any smoking of the solution, and the color of the solution would be unchanged and the MS spectra would not show representative peaks of OPA (SOM/S4). In turn, the synthesis would produce CdSe QDs instead of QRs as seen by TEM studies (SOM/S5). Postoxidation MS data also shows no indication of 1-octene being present at ~112 mass/charge units. Because the generation and rapid decomposition of 1-octene above its autoignition temperature was instantaneous, no dissolved 1-octene was evident in the aliquots. Another important observation is the drastic increase in the DOPA relative abundance in comparison to that of TDPA as mentioned previously. Originally a relative abundance of TDPA:DOPA was 1:0.14, but after the combustion step we see that altered significantly to a ratio of 1:0.8. This is crucial evidence in the understanding of the oxidative route that TOPO takes as illustrated in the Supporting Information.

After the oxidation of TOPO at elevated temperatures and with an applied vacuum, DOPA, OPA, and MOPA formation have been identified. The emergence of MOPA will be discussed below. First, DOPA was produced in the largest quantities as evidenced by the increase in the relative abundance of DOPA from 14 to 80% from pre- and postoxidation samples. DOPA formation should proceed by the oxidation of TOPO at the phosphorus atom by oxygen, the subsequent 1-octene leaving group and proton extraction from residual H_2O to acidify the molecule. Stoichiometric H_2O formation as a product of CdO/TDPA chelation was thoroughly analyzed by Liu et al. and Owen et al. and found to reside in the reaction vessel.[43,51] DOPA is traditionally synthesized in two routes: (1) utilizing 1-octene and hypophosphorous acid (H_2PO_2H) and (2) by oxidizing di-*n*-octylphosphine oxide (DOPO) in the presence of H_2O_2.[52,53] Overall, the mechanistic details of such an oxidation step are very complex and beyond the scope of this present study. We believe that DOPA, in concert with OPA, is of direct importance to the anistropic growth of the CdSe QRs.

After a single alkyl chain was cleaved from the phosphorus atom in TOPO, DOPA was produced first and, as the oxidation continues, the second cleavage in turn produces OPA (Figure 5). OPA was produced in smaller quantities at a relative abundance of 8.7% after the oxidative step of the synthesis (Figure 4B). This is an order of

(51) Owen, J. S.; Park, J.; Trudeau, P. E.; Alivisatos, A. P. *J. Am. Chem. Soc.* **2008**, *130*, 12279.
(52) Peppard, D. F.; Mason, G. W.; Lewey, S. *J. Inorg. Nucl. Chem.* **1965**, *27*, 2065.
(53) Williams, R. H.; Hamilton, L. A. *J. Am. Chem. Soc.* **1952**, *74*, 5418.

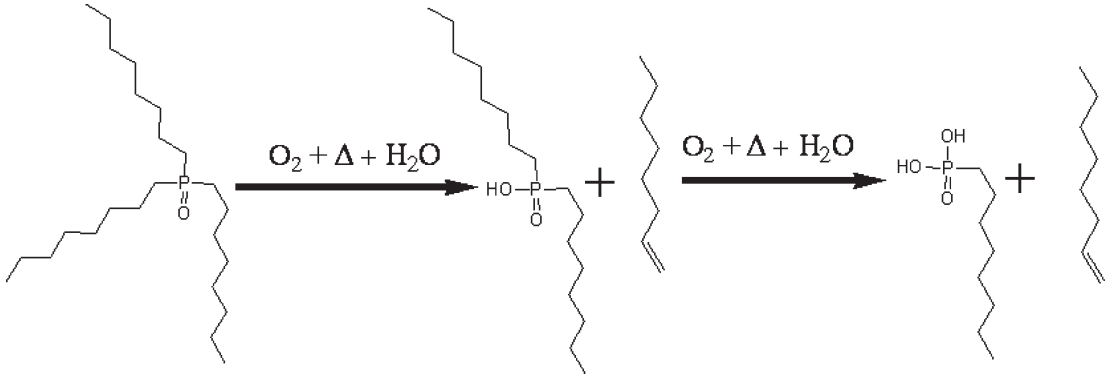

Figure 5. Schematic representation of the oxidation of TOPO into three chemical species: (1) di-*n*-octylphosphonic acid (DOPA), (2) 1-octene, and (3) octylphosphonic acid (OPA). Mono-*n*-octylphosphinic acid was left out for clarity. Specific oxidative mechanisms of TOPO are beyond the scope of the paper, but the general oxidative pathway is reinforced by both MS and NMR spectra. Strict stoichiometry was not enforced in this general mechanism.

magnitude increase over the preoxidation abundance of 0.75% that was detected prior to the oxidation step. This is a reasonable rate of turnover considering DOPA formation is a preceding step in the oxidative pathway toward OPA. In relative abundances, DOPA:OPA has a ratio of 1:0.109, and thus out of approximately 10 available DOPA molecules, 1 OPA molecule is formed. Another molecule formed as a side product in the oxidation of TOPO is MOPA. MOPA was also detected by MS in negative polarity mode at 177.18 mass/charge units (SOM/S6). The relative abundance of MOPA was 1.9%, ca. 20% that of OPA. Although MOPA was a minor product in the oxidative step, MOPA has been identified as aiding in the formation of high-quality CdSe nanowires along with DOPA and OPA.[36]

^{31}P NMR spectroscopy was also utilized to look at the pre and postoxidation solutions to detect any specific signatures of molecular TOPO and its derivatives (Figure 4A, B). The main peak present in the precombustion solution is that of TOPO at 49.2 ppm. Cd-TDPA, which has been previously identified at ~25 ppm, was not readily observed in our study.[49] It has been found that the concentration and molecular makeup of an individual sample can affect ^{31}P peak positions, we conclude that bound Cd-TDPA with TOPO could be lost under the TOPO peak. This discrepancy has not been fully understood up to this point. Control ^{31}P NMR studies of TDPA and chelated Cd-TDPA revealed peaks ranging from 25 to 35 ppm (SOM/S7). Although DOPA was identified via MS prior to the oxidation of TOPO, ^{31}P NMR spectra were unable to readily resolve a representative peak. Postoxidation solutions did reinforce the findings of the MS data and peaks representative of DOPA and OPA were found at 56.2 ppm and 32.5 ppm, respectively. As mentioned by Wang et al. previously, the relative peak shifting of TOPO and phosphinic/phosphonic acids are extremely sensitive to the other molecules present in solution and their relative amounts (see Figure S17 in ref 36).[36,44] Relative molecular ratios were not applied to the case of TOPO:DOPA or TOPO:OPA because of the relatively minute amounts observed. Pre and postoxidation solutions did show a shift of 0.087 ppm in the ^{1}H NMR spectra representative of the protons on the alkyl chains of TOPO (SOM/S8). Overall, the use of MS was more sensitive with the resulting solutions, but we found it necessary to reinforce the presence of DOPA and OPA via an alternative experimental technique.

Historically, the organometallic method using TOPO for CdSe QD and QR synthesis is by far the most widespread, yet the decomposition of TOPO is rarely discussed. Previous investigations in which only certain batches of technical TOPO of varied age produced QRs, was a good indication that phosphonic acids were responsible for anistropic growth. It is possible that the decomposed byproducts of aged TOPO produced over time in open air lab conditions were in fact DOPA, OPA, and MOPA. Although merely conjecture, long-term exposure of TOPO to O_2 and H_2O could result in the oxidation pathway that we highlighted, wherein successive alkyl chains are cleaved as a result of oxidation. In our case, this oxidative process took mere seconds to occur, as opposed to oxidation over a number of months in open air lab conditions. That being said, the long-term storage of TOPO in an inert atmosphere such as a glovebox may be advantageous to reproducible synthesis sensitive to the presence of phosphinic/phosphonic acid byproducts.

Conclusion

Using commercially available high-purity TOPO at elevated temperatures, in the presence of residual oxygen, and an applied vacuum, TOPO was decomposed to DOPA, OPA, and MOPA. With DOPA and OPA in the reaction solvent mixture, CdSe QRs (~4 nm x 20 nm) were synthesized. This finding reinforces the work of Wang et al. in their systematic investigation of DOPA, OPA and MOPA addition and its influence on CdSe 1D nanostructure formation. Prior to the high temperature oxidation step, DOPA was detected as a TOPO impurity in the Cd/TOPO/TDPA solution, but did not contribute to QR formation at that concentration. Postoxidation MS data revealed the formation of additional DOPA, OPA and MOPA to the ligand-monomer solution. Subsequently, this lead to anistropic crystal growth along the 001 crystal axis of the CdSe nanocrystals and QR formation was observed. This chemical/morphological

transformation occurred only in the presence of oxygen that was not removed because of a weak vacuum of <1000 mTorr during the degassing protocol. This study has demonstrated that in situ decomposition of TOPO into DOPA, OPA, and MOPA assists CdSe QR formation and the detailed ligand interaction is important to anistropic nanocrystal growth. Our findings suggest that oxidative products of aged TOPO could lead to the formation of a succession of phosphorus containing acids and thereby influence nanocrystal synthesis.

Acknowledgment. We recognize funding support for the Mass Spectrometry Facility provided by the Thermo Electron Corporation (Seed funds), the W.M. Keck Foundation (Grant 001768), and NIH′s National Center for Research Resources (SIG S10RR020939). A.W. recognizes funding through the Chancellor's Dissertation Year Fellowship at UCSC. The authors would like to thank the National Center for Electron Microscopy at Lawrence Berkeley National Laboratory for the use of its facilities and Tevye R. Kuykendall for assistance with imaging. The authors especially thank Dr. Daniele Gerion and Dr. Natalia Zaitseva for guidance in the synthesis of quantum confined nanostructures. We are grateful to the Basic Energy Sciences Division of the U.S. DOE (05ER4623A00) for financial support.

Supporting Information Available: Additional TEM images of CdSe QDs/bipods/tripods/tetrapods, MS, and NMR spectra of control solutions (PDF). This material is available free of charge at via the Internet at http://pubs.acs.org.